Avicenna J Environ Health Eng. 2018 June;5(1):56-66 http://ajehe.umsha.ac.ir

Original Article

doi 10.15171/ajehe.2018.08

Carbon Modified Pumice as a New Adsorbent for the Rapid Removal of Fluoride Ions From Aqueous Phase

Ghorban Asgari[1], Afsaneh Rafizadeh[2], Maryam Ghasemi[2,3*]

[1]Social Determinants of Health Research Center (SDHRC), Department of Environmental Health Engineering, Hamadan University of Medical Sciences, Hamadan, Iran
[2]Students Research Center, Hamadan University of Medical Sciences, Hamadan, Iran
[3]Young Researchers and Elite Club, Arak Branch, Islamic Azad University, Arak, Iran

***Correspondence to**
Maryam Ghasemi,
Email:
Maryam_ghasemi6282@yahoo.com

Published online D

Abstract
Carbon modified pumice (CP) was successfully synthesized for the rapid removal of fluoride ions from the solvent phase. The batch experiments were conducted to investigate the effect of several operational parameters including carbon content, solution pH, initial fluoride concentration, contact time, adsorbent dose, and temperature on the CP efficiency in fluoride adsorption. The surface morphology, as well as the structural and functional groups of the synthesized CP were evaluated using the scanning electron microscopy (SEM), Brunauer, Emmett and Teller (BET) method, X-ray diffraction (XRD), and Fourier-transform infrared spectroscopy (FTIR), respectively. The adsorption isotherm and kinetic data were found to be in good agreement with the Langmuir and pseudo-second-order models, respectively. Finally, the negative value of ΔG° revealed the spontaneous nature of the fluoride adsorption onto the CP adsorbent.
Keywords: Pumice, Fluoride removal, Carbon, Adsorption isotherm, Drinking water

Received March 3, 2018; **Revised** May 29, 2018; **Accepted** June 25, 2018

1. Introduction

The presence of fluoride in drinking water can be either beneficial or harmful to human health depending on its concentration. According to the World Health Organization (WHO) guidelines, the permissible levels of fluoride in drinking water is 1.5 mg/L (1). The optimum concentration of fluoride is good for dental health and bone development (2). Excessive concentration of fluoride in drinking water can cause dental and skeletal fluorosis, and lesions of the thyroid, liver, and other organs (3). Some fluoride compounds, such as sodium fluoride, fluorspar, fluorapatite, and fluorosilicates easily dissolve in groundwater as they pass through gaps and pores between rocks or soils. In addition, fluoride is found in other sources and fluoridated products such as pesticides, toothpaste, salt, post-harvest fumigants, medications, dental restorations, and health supplements (4). The fluoride present in these kinds of soils, rocks, or sources is substituted by OH− ions under redox conditions, resulting in the release of fluoride ions to the circulating water (5). Several treatment methods including reverse osmosis and membrane processes, ion exchange, coagulation-precipitation, and adsorption have been applied to remove excess fluoride from the drinking water (6). Among these methods, adsorption is the most appropriate process for fluoride removal due to its ease of operation, high efficiency, and low cost (7). The fluoride ion adsorption onto adsorbent consists of three steps: the first step is the diffusion or transport of fluoride ions from bulk solution to the external surface of the adsorbent particle; the second step is the adsorption of fluoride ions onto particle surfaces; and the third step is the fluoride exchange with the structural elements inside adsorbent or transfer of fluoride ions to the internal surfaces of the adsorbent particle (8). Various conventional and non-conventional adsorbents such as aluminum hydroxide coated rice husk ash (5), single- and multi-walled carbon nanotubes (9), MgO nanoparticle loaded mesoporous Al2O3 (10), Mg-Al layered double hydroxides (11), Citrus limonum (lemon) leaf (12), bone char (13), wheat straw, sawdust and activated bagasse carbon of sugarcane (14), and pumice stone (15) have been used for the removal of fluoride ions from drinking water.

Pumice is a light, porous, and volcanic stone with a large surface area. Pumice has attracted considerable interest because of its large surface area, high water adsorption capacity, surfaces with the negative charge, and cost-effectiveness. This volcanic rock has a high silica

content (generally 60%–75% SiO_2), which results in high abrasive characteristics (16). The silica surface consists of silanol groups that extend over the matrix of the silica. The silanol group of the surface is a very active group, which can react with many polar organic compounds and various functional groups (17); thus modified pumice could be a suitable candidate as an adsorbent. Sucrose, as one of the main products of photosynthesis, is regarded as one popular carbon precursor owing to its non-toxicity, biodegradability, and availability. Sucrose serves as a carbon precursor due to its carbon-rich character and the ability of complexation with metal ions. Carbon-coating can function as a reducing agent, avoiding the formation of trivalent phases during sintering of the adsorbent (18,19).

In this work, modification of NP with carbon leads to the increase of specific surface area of pumice. To our knowledge, carbon modified pumice (CP) has not been previously used for the adsorption of fluoride. The prepared adsorbent was characterized using scanning electron microscopy (SEM coupled with EDAX), Brunauer, Emmett and Teller method (BET), X-ray diffraction (XRD), and Fourier-transform infrared spectroscopy (FTIR). Then the removal of fluoride from drinking water was well investigated and elucidated using the batch method and the uptake of fluoride onto CP was considered for its equilibrium, kinetics, and thermodynamic studies.

2. Materials and Methods

2.1. Preparation of Carbon/Pumice

The natural pumice (NP) stone was collected from Tikmadash mine in the south of East Azerbaijan province located in the northwest of Iran, where such mines are abundantly available. Pumice samples were washed with distilled water several times to remove the impurities. The samples were then dried out at room temperature. Afterward, the stone was crushed and sieved through No. 80 and 100 mesh size sieves.

In addition, pumice and various amounts of sucrose (containing 0.25-1 mol/L of sucrose solution) were dissolved in distilled water in order to modify the surface of NP with carbon and then, the mixture was dried under air at 90°C for 12 hours to obtain sucrose/pumice precursors. Next, the precursors were heated at room temperature to 500°C at a rate of 2°C/min and kept at this temperature for 4 hours in the presence of nitrogen gas. Finally, carbon/pumice (CP) was ground and sieved under 120 mesh (125 μM) size (19).

2.2. The Characterization of Carbon/Pumice

The natural and prepared CP were characterized by means of various instrumental techniques including the XRD, BET method, SEM, and FTIR. Further, the surface mineralogical composition of NP and CP were determined by an X-ray diffractometer (Philips APD-3720) at the scanning range of 2θ=5-80°. Furthermore, the morphology and other surface characteristics of the NP and CP were characterized by SEM coupled with energy dispersive detector (EDAX, SEM, S-4160, Hitachi, Japan). Moreover, the specific surface area of the adsorbents was tested from the N_2 adsorption/desorption method according to the BET isotherm model (Belsorp-max, Japan) at liquid nitrogen temperature (77 K). Eventually, the surface chemical properties of NP and CP were determined by Fourier transform infrared spectroscopy (FTIR, FDU-3, DR-11) in the wave number ranging from 400 to 4000 cm^{-1}.

2.3. Reagents

All the used chemicals and reagents were of analytical reagent grade. NaF and sucrose, as well as ammonium hydroxide were purchased from Merck Company (Germany). Additionally, the required concentration of the fluoride solution was prepared using the stock solution. Ultimately, the initial pH of the solution was regulated by adding 0.1 mol/L HCl or 0.1 mol/L NaOH solutions.

2.4. Adsorption Experiments

Adsorption experiments were performed in 1000 mL conical flask by dispersing 0.5 g of the adsorbent with 500 mL of the fluoride solution at room temperature. The primary concentration of the fluoride solution was 10 mg/L and the mixture was placed in a mechanical shaker for 60 minutes. The effect of the initial pH of the solution on fluoride adsorption was determined by various pH ranging from 3 to 11. In addition, the effect of adsorbent dosage on fluoride adsorption was investigated by varied adsorbent doses from 0.2 to 2 g/L of CP. Then, 500 mL of the fluoride solution was added to 0.5 g of the CP in order to test the isotherm. The primary concentrations of the ions were 5–25 mg/L for 2 hours to obtain equilibrium. Further, 500 mL of 10 mg/L fluoride solution was added to 0.5 g of the CP at different times in order to test the kinetic (10-60 minutes). The thermodynamic parameters were evaluated at different temperatures (i.e., 298, 308, 318, and 328 K) and the primary concentration of the fluoride was 10 mg/L. Adsorption studies were performed at the shaking speed of 100 rpm inside a shaker incubator container. After ending the contact time, the samples were centrifuged at 4000 rpm for 10 minutes and then were filtered through a filter paper and finally, the residual fluoride concentration was analyzed. Furthermore, the residual fluoride concentration in the aqueous solution was determined by using a UV/Vis spectrophotometer. The adsorption capacity (q_e) and the removal efficiency (%RE) of the fluoride ions by CP were expressed by the following equations:

$$q_e(mg/g) = \frac{C_0 - C_e}{m} \times V \quad (1)$$

$$\%RE = \frac{C_0 - C_e}{C_0} \times 100 \quad (2)$$

where, C_0 (mg/L) and C_e (mg/L) represent the concentration of the fluoride ion before and after the adsorption tests, respectively. Moreover, q_e, V (L), and m (g) denote the adsorption capacity of the fluoride ion, the solution volume of the ion, and the amount of CP, respectively.

2.5. Determination of pH_{zpc} of CP

The zero point charge (ZPC) was determined using 0.01 M solution of NaCl as an electrolyte and by adding 0.1 M solutions of NaOH or HCl. For this purpose, the pH of 6 beakers containing 500 mL of the electrolyte was set to the desired values in the range of 2-12. After ending the contact time, the suspensions were filtered through the filter paper, and the final pH values of each beaker were measured.

2.6. Kinetic Studies

The kinetics of the fluoride adsorption on the CP adsorbent was analyzed by the integrated pseudo-first-order (Eq. 3), pseudo-second-order (Eq. 4), and intra-particle diffusion (Eq. 5) models (20-22) as follow:

$$\log(q_e - q_t) = \log q_e - \frac{k_1 t}{2.303} \quad (3)$$

$$\frac{t}{q_t} = \frac{1}{k_2 q_e^2} + \frac{1}{q_3} t \quad (4)$$

$$q_t = k_i t^{0.5} + I \quad (5)$$

where, q_e and q_t are the adsorption capacity at equilibrium (mg/g) and the adsorption capacity at the time of t (mg/g). Additionally, k_1, k_2, k_i demonstrate the first-order rate constant (1/min), the second order rate constant (g/mg·min), and the intra-particle diffusion rate constant (mg/g·$min^{0.5}$), respectively. The values of pseudo-first-order (q_e and k_1) and pseudo-second-order (q_e and k_2) kinetic constants are experimentally defined from the slope and intercept of the linear plots of the log (q_e-q_t) versus t, as well as the slope and intercept of the linear plots of t/q_t versus t, respectively. In addition, the values of intra-particle diffusion constants (k_i and I) are described from the slope and intercept of the linear plots of q_t versus $t^{0.5}$, respectively.

The validity of the kinetic models was determined based on the normalized standard deviation (NSD) and average relative error (ARE), which was calculated according to Eqs. (6) and (7):

$$\mathrm{NSD} = 100\sqrt{\frac{1}{N-1}\sum_{i=1}^{N}\left[\frac{q_t^{exp} - q_t^{cal}}{q_t^{exp}}\right]^2} \quad (6)$$

$$\mathrm{ARE} = \frac{100}{N}\sum_{i=1}^{N}\left|\frac{q_{e,exp} - q_{e,cal}}{q_{e,exp}}\right|_i \quad (7)$$

where, $q_{e,exp}$ is the observation from the batch experiment i and $q_{e,cal}$ is estimated by the kinetic for the corresponding $q_{e,exp}$. In addition, N denotes the number of observations in the obtained measurements (15, 23).

2.7. Isotherm Studies

Langmuir, Freundlich, and Dubinin Radushkevich (D-R) isotherm models were applied to describe the isotherm of the fluoride adsorption on CP adsorbent.

The Langmuir model (24) expresses the monolayer coverage of the fluoride ions on the outer surface of the CP sorbent without any interactions. The Langmuir isotherm was obtained by the following equations:

$$\frac{C_e}{q_e} = \frac{1}{q_m K_L} + \frac{C_e}{q_m} \quad (8)$$

where, q_m is the maximum adsorption capacity (mg/g) and K_L represents the Langmuir constant (L/mg) which relates to the energy of adsorption. Further, the values of q_m and K_L are determined from the slope and intercept of the linear plots of C_e/q_e versus C_e, respectively.

The important feature of the Langmuir model can be described based on the dimensionless constant R_L parameter expressed by Eq. (9):

$$R_L = \frac{1}{1 + K_L C_0} \quad (9)$$

The R_L value confirms that the adsorption is favorable ($0 < R_L < 1$), unfavorable ($R_L > 1$), linear ($R_L=1$), or irreversible ($R_L=0$) (25).

Furthermore, the Freundlich model (26) indicates the adsorption of the fluoride ions on a heterogeneous surface of CP with different site energies. The Freundlich isotherm is expressed in the following linear form:

$$\log q_e = \log K_F + \frac{1}{n}\log C_e \quad (10)$$

where, K_F demonstrates the bonding energy constant (mg/g) and n is the Freundlich exponent related to the adsorption intensity (dimensionless). The values of n and K_F were estimated from the slope and intercept of the linear plots of log q_e versus log C_e, respectively.

The D-R (27) model was used to express the adsorption mechanism onto a heterogeneous surface of CP. The D-R isotherm is expressed in the following linear form:

$$\ln q_e = \ln Q_m - K_D \varepsilon^2 \quad (11)$$

where, ε is the Polanyi potential which is calculated by the following equation:

$$\varepsilon = RT \ln\left(1 + \frac{1}{C_e}\right) \quad (12)$$

in which, K_D and Q_m represent a constant related to the adsorption energy (mol^2/kJ^2) and the adsorption capacity (mg/g), respectively. Additionally, R and T are the gas constant and temperature (8.314 J/mol.K and K). The values of Q_m and K_D were determined from the slope and intercept of the linear plots of ln q_e versus ε, respectively. The mean free energy of adsorption (E) can be calculated using the following equation:

$$E = \frac{1}{\sqrt{2K_D}} \quad (13)$$

In addition, the validity of the isotherm models was determined based on the root mean square error (RMSE) and the chi-square test (X^2) which can be described as:

$$RMSE = \sqrt{\frac{1}{N-2}\sum_{i=1}^{N}(q_e^{\exp} - q_e^{cal})^2} \quad (14)$$

$$X^2 = \sum_{i=1}^{n}\frac{(q_e^{\exp} - q_e^{cal})^2}{q_e^{cal}} \quad (15)$$

where, $q_{e,exp}$ is the observation from the batch experiment and $q_{e,cal}$ denotes the estimated from the isotherm for the corresponding $q_{e,exp}$. Further, N indicates the number of observations in the obtained measurements (28).

2.8. Thermodynamics Studies

The Gibbs free energy change (ΔG°), enthalpy (ΔH°), and entropy (ΔS°), as the symptoms of a thermodynamic process (25), were calculated using the following equation:

$$\Delta G^{\circ} = -RT\ln\frac{q_e}{C_e} \quad (16)$$

$$\ln\frac{q_e}{C_e} = \frac{\Delta S^0}{R} - \frac{\Delta H^0}{RT} \quad (17)$$

where, R and T are the universal gas constant (8.314 J/mol.K) and absolute temperature (K).

3. Results and Discussion

3.1. Adsorbent Characterization

The SEM images of the NP and CP are displayed in Figs. 1a and b, respectively. The surface of the NP shows irregular texture with sharper edges while CP demonstrates deep channels and cavities with a smooth surface. This structure is responsible for increasing the fluoride ion sorption capacity. The results of the chemical composition of the NP and CP obtained from the SEM coupled with energy dispersive analysis of the X-ray (EDAX) are presented in Table 1. Based on the results, the SiO_2 is detected as the major constituents of NP while other elements are present in relatively smaller amounts. After the modification, the presence of carbon is observed to increase from 0.01% to 45.92%. Furthermore, the specific surface area and pore volume of NP and CP are 2.12 m^2/g, 0.0062 cm^3/g, as well as 250.813 m^2/g, 0.0255 cm^3/g, respectively. Moreover, the results indicate that the specific surface area and pore volume of NP is increased after modification with carbon, resulting in an increase in the fluoride ion sorption onto CP. Fig.s 2a and b depict the adsorption-desorption isotherms of N_2 at 77 K of CP adsorbent and the differential pore size distribution calculated by the BJH method. Additionally, the curve model is of type I isotherm with a hysteresis loop due to the mesoporous structure (2-50 nm).

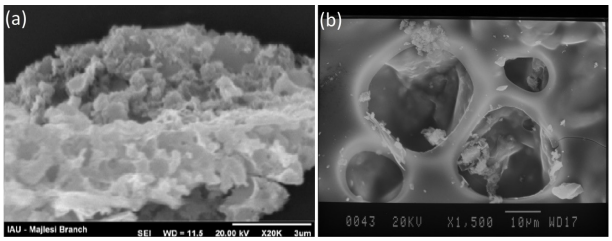

Fig. 1. The SEM Images of (a) NP and (b) CP.
Note. NP: Natural pumice; CP: Carbon modified pumice; SEM: Scanning electron microscopy.

The XRD patterns of the NP and CP adsorbents are illustrated in Fig. 3. The peaks at 2θ=20-40° can be considered the evidence for the presence of some amorphous phases in both adsorbents. The decrease in the height of the dome (i.e., 2θ=20 and 40°) in the modified adsorbent can be attributed to a decrease in the

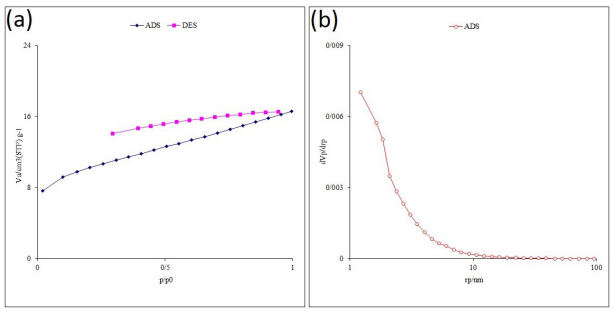

Fig. 2. (a) N_2 Adsorption-Desorption Isotherms and (b) Pore Size Distribution of CP. Abbreviation: CP, Carbon modified pumice.

Table 1. The Elemental Composition (by wt.%) of NP and CP Obtained From the EDAX Characterization

Elements	% C	% O	% Si	% Al	% K	% Na	% Ca	% Fe
NP	0.01	66.49	24.29	5.75	1.07	0.91	0.89	0.58
CP	45.92	42.24	8.91	1.61	0.36	0.34	0.21	-

Abbreviations: NP, Natural pumice; CP, Carbon modified pumice; EDAX, electron microscopy coupled with energy dispersive analysis of the X-ray.

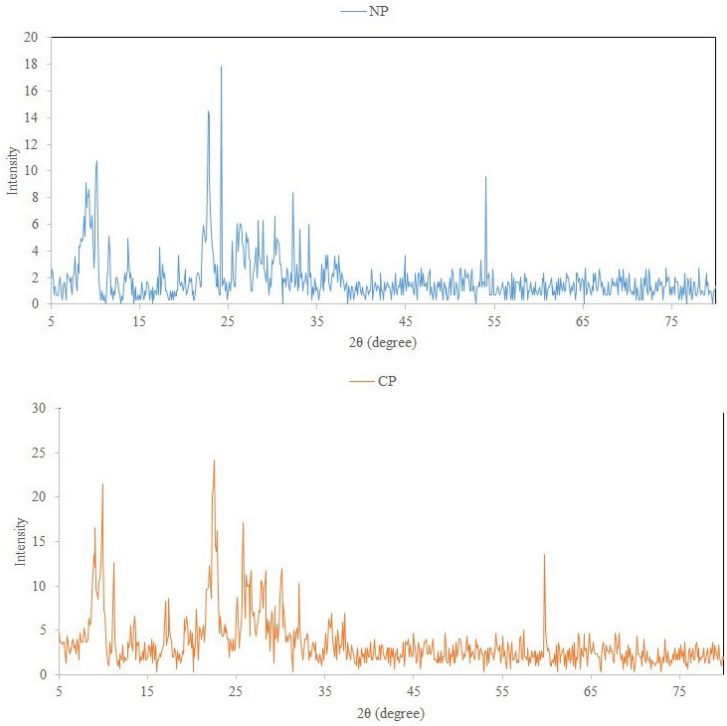

Fig. 3. The XRD Patterns of (a) NP and (b) CP. Abbreviation: XRD, X-ray diffraction; NP, Natural pumice; CP, Carbon modified pumice.

amorphous phase in CP.

Fig. 4 shows the FTIR spectra in the range of 4000-400 cm^{-1} of NP, CP, and CP after the adsorption process. NP sample indicates strong bands at 475, 620, 799, and 1085 cm^{-1} assigned to the stretching vibrations and bending modes of the Si-O and Al-O bonds, as well as the Si-O-Al stretching vibration for NP, CP, and CP after the adsorption process (4, 29). In addition, the peak at 1650 cm^{-1} can be ascribed to the bending vibration of the H-O-H bond (16). The bands at 3470 cm^{-1} belong to the stretching vibration of H_2O molecules (moisture). As can be observed, after modification, the new peak at 2930 cm^{-1} is related to the C-H stretching vibration, indicating that the amino- carbon group is successfully grafted onto the NP. Further, the FTIR spectrum of CP indicates the changes after the adsorption process. These shifts in peak frequencies represent that binding processes are taking place on the surface of CP.

3.2. The Effect of Carbon Content

The removal efficiency of CP in deionized water as a function of carbon content was studied by varying the sucrose amount from 0.25 to 1.0 wt% (Fig. 5). Maximum removal efficiency (97%) was obtained at 0.5 wt% of

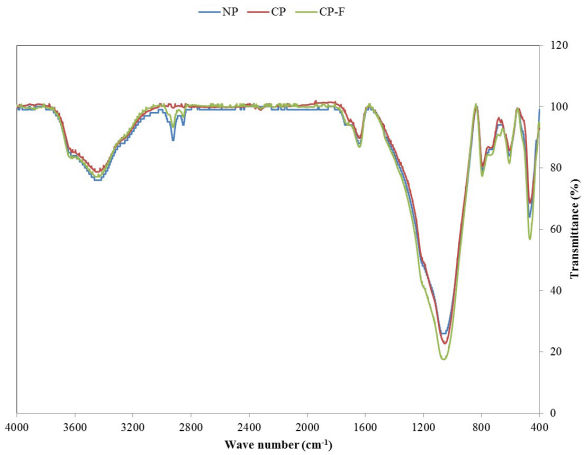

Fig. 4. The FTIR Spectra of NP, CP, and CP After Fluoride Adsorption. *Abbreviation:* FTIR, Fourier Transform Infrared analysis; NP, Natural pumice; CP, Carbon modified pumice.

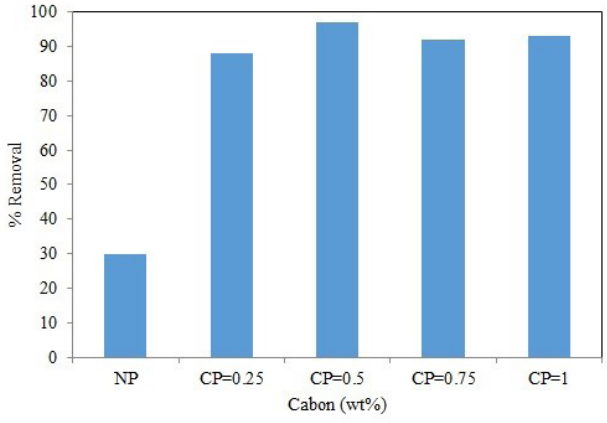

Fig. 5. The Effect of Carbon Content on the Removal of the Fluoride Ion. *Note.* Condition: Dose of NP: 10 g; Volume of the sucrose solution: 200 mL; The concentration of the sucrose solution: 0.25-1 mol/L.

carbon, which was extremely higher than that of the NP adsorbent. Asgari et al (15) and Ersoy et al (30) reported that NP had a negative charge and thus the fluoride ion was repelled by the negatively charged NP surface since this ion had a negative charge. Accordingly, the surface of NP was modified with carbon in order to increase the removal efficiency, which neutralized the negative charges. Furthermore, the initial increment in the removal efficiency may be attributed to an increase in the micropore content and the number of active sites on the CP, which promoted the development of mesopores on the NP surface (31). As a result, considering the increase in the sucrose content, the internal and external surface of the CP was uniformly covered and the specific surface area gradually decreased (29). Therefore, the optimum sucrose amount was 0.5 wt% and the remaining tests were evaluated using this adsorbent.

3.3. The Effect of pH

The effect of solution pH on the fluoride removal efficiency of the CP was studied in the pH range of 3-11 (Fig. 6). As shown in Fig. 6b, the maximum fluoride removal efficiency of the CP at a pH value of 7 is 97% and then, it decreases while raising the pH from 7 to 11. This behavior is attributed to the electrostatic interactions between the fluoride ions in the aqueous solution and the surface charge of the CP adsorbent. The surface of CP is negatively charged when the pH value is above the pH_{ZPC} while it is positively charged when the pH value is below the pH_{ZPC}. The pH_{ZPC} of the CP is 6.4 which is in line with the results of several other studies regarding the CP (2,4,32). Therefore, the fluoride ions in the solution are attracted to the surface of CP sorbent at $pH < pH_{ZPC} = 6.4$ and there is a competition between the hydroxyl groups and fluoride ions for the sorbent active sites since the surface sites are positively charged (8). Moreover, the mechanisms involved in the removal efficiency of an anionic adsorbate (e.g., the fluoride ions) by an adsorbent (e.g., the CP sorbent) may be through the specific and/or non-specific adsorption processes. The specific adsorption involves ligand/anion exchange reactions where the anions displace OH^- and/or H_2O from the sorbent surface. However, the non-specific adsorption includes Columbic forces of the attraction between the anion and the adsorbent and mainly depends on the pHpzc of the sorbent (2,33). The lower fluoride removal efficiency of the CP below pH 6 could be due to the reduced availability of free fluoride ions due to the formation of the weak hydrofluoric acid while the reduction at high pH may be due to the competitive interaction with hydroxyl ions (9,34). Additionally, according to Ersoy et al (30), the inverse relationship between pH and zeta potential demonstrates the adsorption process by the Coulombic interaction. This interaction may be due to the presence of $\equiv Si^+$ and $Si\text{-}OH_2^+$ groups which emerge during the grinding process as a result of bond breaking or the deprotonation of ≡Si-OH groups at the particles surface of the pumice materials (4). The predicted mechanism of the fluoride adsorption under acidic conditions is mainly corroborated with the following equation:

$$\equiv MOH + H2O + F^- \leftrightarrow MOH_2^+ + F^- + OH^-$$
$$\leftrightarrow MOH_2^+ \ldots F^- + OH^-$$
$$\leftrightarrow M{-}F + H2O + OH^-$$

where, M=Al or Si.

The decrease in the fluoride removal from 97 to 91% under alkaline conditions (pH 9-11) may be due to the excess of the competition of hydroxyl ions with fluoride ions for the active sites on the CP sorbent and/or the electrical repulsion between negatively charged CP surface sites and fluoride ions. Therefore, the optimum pH is 7 and the remaining examinations are evaluated at this optimum pH.

3.4. The Effect of Adsorbent Dosage

The effect of the adsorbent dosage on the removal efficiency of the fluoride was evaluated with a fixed fluoride concentration of 10 mg/L, the results of which are provided in Fig. 7a. As shown, the fluoride removal efficiency increases from 75 to 96% when the adsorbent dosage increases from 0.2 to 2 g/L because of the greater surface area and the availability of more active adsorption sites at a higher adsorbent dosage (35). In addition, there

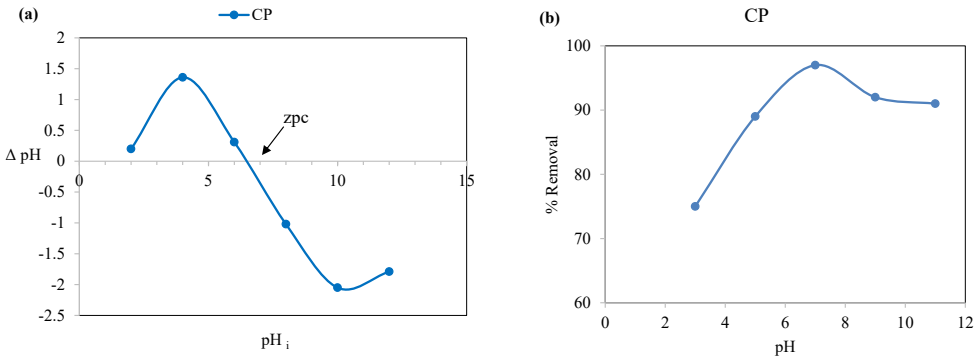

Figure 6. (a) pH_{ZPC} Draft and (b) the Effect of pH on the Removal of the Fluoride Ion.

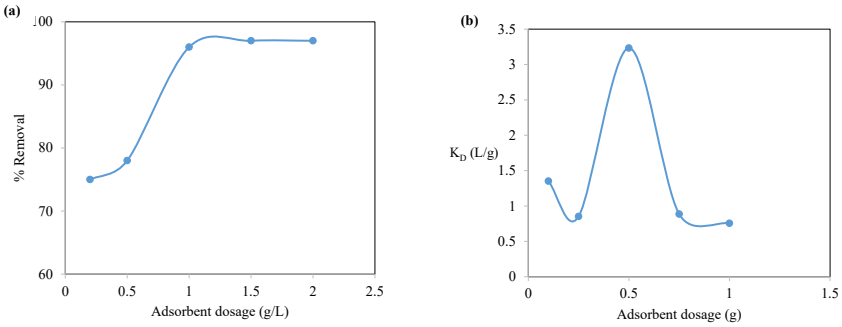

Fig. 7. (a) The Effect of CP Dose on the Removal of the Fuoride Ion and (b) K_D Draft. Abbreviations: CP, Carbon modified pumice.

is no significant change in the removal efficiency of the fluoride in more than 1 g/L of adsorbent that may be due to the overlapping of the active adsorption sites at a higher dosage, as well as a decrease in the effective surface area resulting in the conglomeration of the exchanger particles (4,36). In the current study, the fluoride level was reduced from the initial concentration of 10 to 1 mg/L by the 0.5 g (1 g/L) of CP. Since the permissible limit for the fluoride in drinking water is fixed at 1.0 mg/L, it is concluded that only a maximum of 0.5 g of the CP is needed for the efficient removal of the fluoride from the water.

The distribution coefficient namely, K_D reflects the binding ability of an adsorbent surface for a solute. Further, K_D is a ratio of the solute concentration in the solid and aqueous phases and the value of K_D for a given system mainly depends on solution pH and the type of adsorbent surface. The K_D values for the fluoride on CP were calculated using the following relationship:

$$K_D = q_e/C_e \quad (18)$$

where, q_e (mg/g) and C_e (mg/L F^-) are the solute concentration in the solid adsorbent and aqueous phase at equilibrium, respectively. In the present study, an increase in K_D values with the increase in the adsorbent dosage (Fig. 7b) indicate that the binding ability of the surface reduces with an increase in the adsorption density and heterogeneous surface of the adsorbent (2,4). According to the surface site heterogeneity model, all types of active sites are entirely exposed to sorption and the surface may become saturated faster at low adsorbent dosages. However, at higher adsorbent dosages, the availability of higher energy sites may decrease and a larger fraction of lower energy sites may be occupied (37).

3.5. The Kinetics of Adsorption

Fig. 8a illustrates the plot of the percentage removal of the fluoride by varying the contact time at 298 K and at pH 7 by the CP surface. The adsorption is not an instantaneous process and the adsorbate (i.e., fluoride

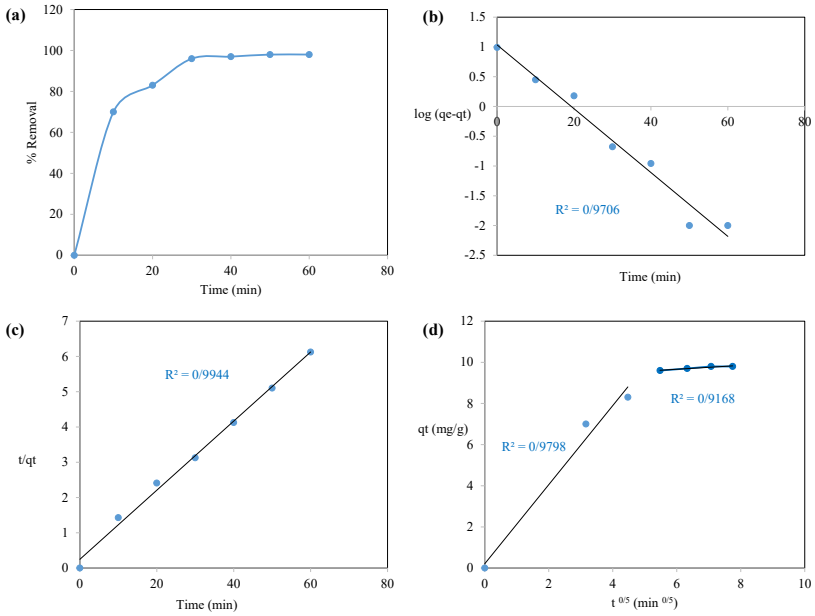

Figure 8. (a) The Effect of Contact Time on the Removal of the Fluoride Ion, (b) Pseudo-First-Order Kinetic Plot, (c) Pseudo-Second-Order Kinetic Plot, and (d) Intraparticle Diffusion Plot. *Note*. Condition: 25°C; 100 rpm; 500 ml of 10 mg/L of the fluoride solution; pH=7.0; 0.5 g of CP.

ions) should first diffuse into the bulk solution through various diffusion mechanisms to available active surface sites on the CP adsorbent for attachment (2). The fluoride adsorption is found to be rapid at the first 10 minutes of the contact where 70% of the equilibrium adsorbed amount occurs by the CP adsorbent. Furthermore, the remaining adsorption occurs by 60 minutes more contact time. The initial rapid removal of the fluoride is presumably due to the instantaneous utilization of the most readily available active sites and ion exchange with surface hydroxyl ions of the outer surface CP adsorbent, the later stage is due to the gradual uptake of fluoride into the inner surface of the porous adsorbent for adherence.

As displayed in Fig.s 8b-d, the obtained data, fit with all three models and all parameters are listed in Table 2. Based on the results, the pseudo-second-order model better fits the experimental data with higher R^2 while lower ARE and NSD compared to the pseudo-first-order model. As it is revealed in the kinetic data, $q_{e,cal}$ value is very close to $q_{e,exp}$, which confirms the high correlation between the experimental data and the pseudo-second-order model. Moreover, there are several steps in the plot drawn for fluoride adsorption by CP adsorbent in the kinetic plot of qt versus $t^{1/2}$. Accordingly, different adsorption mechanisms (e.g., film and intraparticle diffusion) are possibly involved in the adsorption of the fluoride onto the CP adsorbent. Additionally, the initial region of the plot indicates that the surface diffusion (i.e., the boundary layer diffusion) probably limits the fluoride adsorption onto the CP adsorbent at the beginning of reaction time while the second region represents the occurrences of intra-particle or pore diffusion as the adsorption-limiting step.

Table 2. The Kinetic Constants for the Adsorption of Fluoride on CP

Model	Parameter	Unit	Value
Pseudo-first-order	$q_{e,cal}$	(mg/g)	9.81
	$q_{e,exp}$	(mg/g)	10.82
	k_1	1/min	0.123
	R^2	-	0.97
	ARE	-	3.81
	NSD	-	1.333
Pseudo-second-order	$q_{e,cal}$	(mg/g)	9.81
	$q_{e,exp}$	(mg/g)	10.20
	k_2	g/mg.min	0.038
	R^2	-	0.994
	ARE	-	1.56
	NSD	-	0.546
Intraparticle diffusion	$k_{i,1}$	$mg/g.min^{0.5}$	1.922
	I_1	mg/g	0.208
	R^2	-	0.979
	$K_{i,2}$	$mg/g.min^{0.5}$	0.093
	I_2	mg/g	9.10
	R^2	-	0.916

Abbreviation: CP, Carbon modified pumice; ARE, average relative error; NSD, Normalized standard deviation.

3.6. The Isotherm of Adsorption

Fig. 9 and Table 3 demonstrate the plotted and fitted models, as well as the parameters of the fitted isotherms and the correlation coefficient (R^2) in the fluoride adsorption, respectively. As shown, the adsorption of fluoride onto CP adsorbent fits with the Langmuir model with the highest values of the correlation coefficient (R^2=0.988) compared to other fitted isotherms. According to these results, adsorption of fluoride occurs on a homogeneous surface and on a monolayer as expected in the formulation of the Langmuir isotherm onto CP surface. In addition,

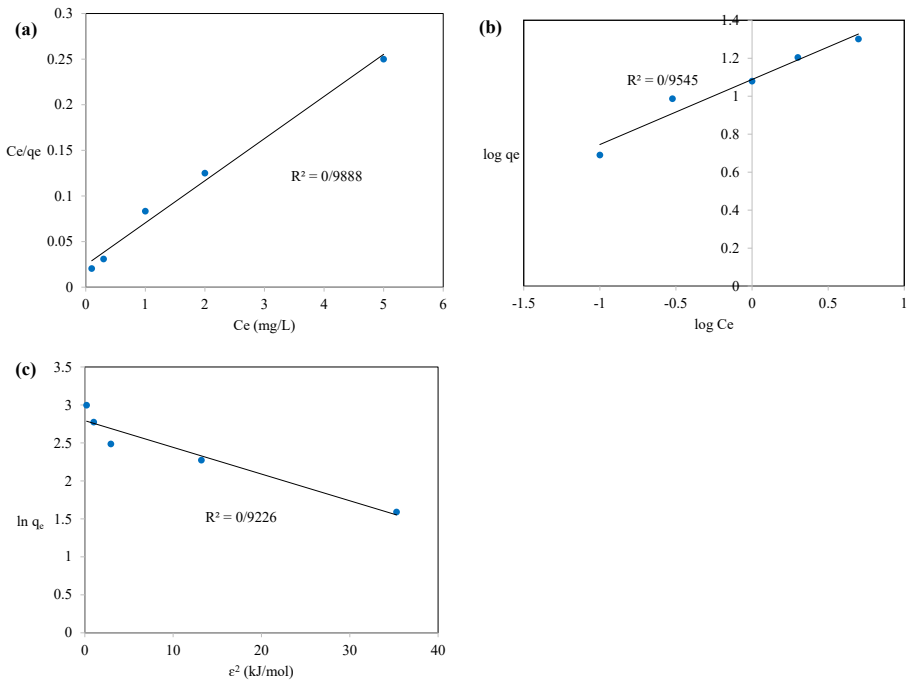

Fig. 9. (a) Langmuir Isotherm Plot, (b) Freundlich Isotherm Plot, and (c) Dubinin–Radushkevich Isotherm Plot.

Table 3. The Adsorption Isotherms of the Fluoride Ion

Model	Parameter	Values
Langmuir	K_L	1.901
	q_m	21.645
	R^2	0.988
	R_L	0.045
	RMSE	0.949
	X^2	0.125
Freundlich	K_F	12.248
	1/n	0.342
	R^2	0.954
	RMSE	4.475
	X^2	4.906
Dubinin–Radushkevich	K_D	0.0352
	Q_m	16.331
	E	3.773
	R^2	0.922
	RMSE	2.118
	X^2	0.824

Abbreviation: RMSE, Root mean square error.

the maximum adsorption capacity for the fluoride ion is found to be 21.645 mg/g. Further, the value of R_L is in the range of 0-1 (0.045) which confirms the favorable uptake of fluoride ions onto CP surface. Finally, the 1/n value is equal to 0.342 which indicates the favorable sorption process in the range of the studied concentrations (0 <1/n <1).

3.7. The Thermodynamics of Adsorption

The effect of temperature on the percentage removal of the fluoride ion on CP was investigated at four different temperatures (i.e., 298, 308, 318, and 328 K) and the results are shown in Fig. 10a. Based on the results, the percentage removal of the fluoride ion decreases from 97% to 89.2% with an increase in the temperature from 298 to 328 K, which indicate that the fluoride ion removal on CP from the aqueous solution is an exothermic process in nature.

A linear plot of ln q_e/C_e versus 1/T is displayed in Fig. 10b. The values of ΔG^o at 298, 308, 318, and 328 K are calculated and observed as -6.89, -6.36, -4.09, and -3.86 kJ/mol (Table 4) which confirm that the adsorption of fluoride ion onto CP is spontaneous and thermodynamically favorable. Furthermore, the values of ΔH^o and ΔS^o are 55.45 kJ/mol and -0.166 kJ/mol.K, respectively. Moreover, the positive value of the enthalpy change represents that the adsorption process is endothermic and the forces involved in the sorption process can be of chemical forces (27). Ultimately, the negative value of the entropy change demonstrates a decline in the mobility freedom of the fluoride.

3.8. The Comparison of Various Adsorbents

The maximum adsorption capacity of CP, along with the equilibrium time for the removal of the fluoride ion was compared with other adsorbents reported in the literature (2,4,6,9,10,15,35,38,39), the values of which are shown in Table 5.

4. Conclusion

In general, the CP was successfully synthesized from pumice and sucrose as the carbon precursors and used to remove the fluoride ions from an aqueous solution. Additionally, the kinetics of the adsorption was explained using the pseudo-second-order model, which was further supported by a significant correlation between the experimental and calculated results. In addition, the Langmuir isotherm was proved to be the best isotherm for modeling the adsorption of the fluoride ions. Eventually, the maximum adsorption capacity of the fluoride onto the CP adsorbent was calculated 21.64 mg/g.

Table 4. Thermodynamic Parameters for the Adsorption of the Fluoride on CP

ΔH° (kJ/mol)	ΔS° (kJ/mol.K)	ΔG° (kJ/mol)			
		298 K	308 K	318 K	328 K
55.45	-0.166	-6.89	-6.36	-4.09	-3.86

Abbreviations: CP, Carbon modified pumice; ΔGo, Gibbs free energy change; ΔHo, Enthalpy; ΔSo, Entropy.

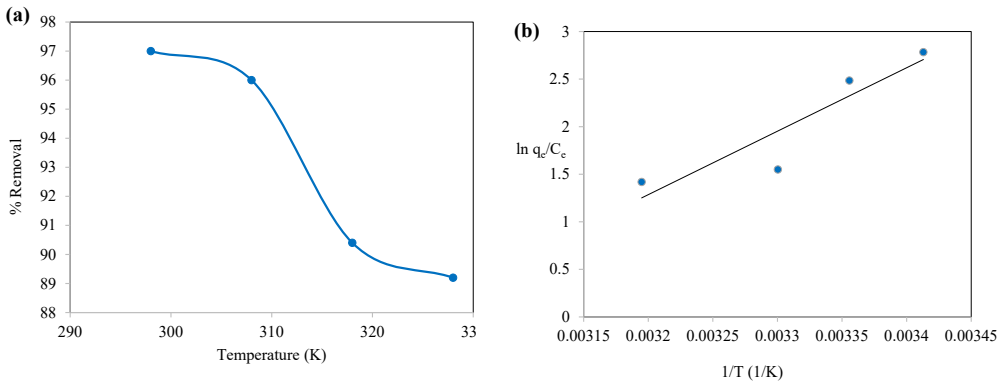

Figure 10. (a) The Effect of Temperature on the Removal of the Fluoride Ion and (b) the Linear Plot of ln q_e/C_e Versus 1/T

Table 5. The Comparison of the Maximum Adsorption Capacity (q_m) of the Fluoride Onto Various Adsorbents

Adsorbent	q_m (mg/g)	Equilibrium Time (min)	Ref.
Iron nano-impregnated black tea	2.18	50	[38]
Single-walled carbon nanotubes	2.4	60	[9]
Hydroxyapatite	3.12	-	[35]
Aluminum oxide coated pumice	7.6	300	[2]
Magnesium chloride modified pumice	11.765	210	[4]
MgO nanoparticle loaded alumina	37.35	600	[10]
Hexadecyltrimethyl ammonium-modified pumice	41.65	40	[15]
Corn stover biochar	6.42	3600	[39]
Magnetic corn stover biochar	4.11	3600	[39]
Hydrous ferric oxide doped alginate beads	8.90	250	[6]
CP	21.645	30	Present study

Abbreviation: CP, Carbon modified pumice.

Conflict of Interest Disclosures

The authors declare that they have no conflict of interests.

Acknowledgements

The authors are thankful to the School of Health, Hamadan University of Medical Sciences, Hamadan, Iran (grand No. 9503271436).

References

1. World Health Organization (WHO). Guidelines for drinking-water quality: incorporating 1st and 2nd addenda, Vol.1, recommendations. 3rd ed. Geneva, Switzerland: WHO; 2008.
2. Salifu A, Petrusevski B, Ghebremichael K, Modestus L, Buamah R, Aubry C, et al. Aluminum (hydr)oxide coated pumice for fluoride removal from drinking water: Synthesis, equilibrium, kinetics and mechanism. Chem Eng J. 2013;228:63-74. doi: 10.1016/j.cej.2013.04.075.
3. Mariappan R, Vairamuthu R, Ganapathy A. Use of chemically activated cotton nut shell carbon for the removal of fluoride contaminated drinking water: Kinetics evaluation. Chin J Chem Eng. 2015;23(4):710-21. doi: 10.1016/j.cjche.2014.05.019.
4. Noori Sepehr M, Sivasankar V, Zarrabi M, Senthil Kumar M. Surface modification of pumice enhancing its fluoride adsorption capacity: An insight into kinetic and thermodynamic studies. Chem Eng J. 2013;228:192-204. doi: 10.1016/j.cej.2013.04.089.
5. Ganvir V, Das K. Removal of fluoride from drinking water using aluminum hydroxide coated rice husk ash. J Hazard Mater. 2011;185(2-3):1287-94. doi: 10.1016/j.jhazmat.2010.10.044.
6. Sujana MG, Mishra A, Acharya BC. Hydrous ferric oxide doped alginate beads for fluoride removal: Adsorption kinetics and equilibrium studies. Appl Surf Sci. 2013;270:767-76. doi: 10.1016/j.apsusc.2013.01.157.
7. Bhatnagar A, Kumar E, Sillanpaa M. Fluoride removal from water by adsorption--a review. Chem Eng J. 2011;171(3):811-40. doi: 10.1016/j.cej.2011.05.028.
8. Mohapatra M, Anand S, Mishra BK, Giles DE, Singh P. Review of fluoride removal from drinking water. J Environ Manage. 2009;91(1):67-77. doi: 10.1016/j.jenvman.2009.08.015.
9. Dehghani MH, Haghighat GA, Yetilmezsoy K, McKay G, Heibati B, Tyagi I, et al. Adsorptive removal of fluoride from aqueous solution using single- and multi-walled carbon nanotubes. J Mol Liq. 2016;216:401-10. doi: 10.1016/j.molliq.2016.01.057.
10. Dayananda D, Sarva VR, Prasad SV, Arunachalam J, Parameswaran P, Ghosh NN. Synthesis of MgO nanoparticle loaded mesoporous Al2O3 and its defluoridation study. Appl Surf Sci. 2015;329:1-10. doi: 10.1016/j.apsusc.2014.12.057.
11. Kameda T, Oba J, Yoshioka T. Recyclable Mg–Al layered double hydroxides for fluoride removal: Kinetic and equilibrium studies. J Hazard Mater. 2015;300:475-82. doi: 10.1016/j.jhazmat.2015.07.023.
12. Tomar V, Prasad S, Kumar D. Adsorptive removal of fluoride from aqueous media using Citrus limonum (lemon) leaf. Microchem J. 2014;112:97-103. doi: 10.1016/j.microc.2013.09.010.
13. Medellin-Castillo NA, Leyva-Ramos R, Padilla-Ortega E, Perez RO, Flores-Cano JV, Berber-Mendoza MS. Adsorption capacity of bone char for removing fluoride from water solution. Role of hydroxyapatite content, adsorption mechanism and competing anions. J Ind Eng Chem. 2014;20(6):4014-21. doi: 10.1016/j.jiec.2013.12.105.
14. Yadav AK, Abbassi R, Gupta A, Dadashzadeh M. Removal of fluoride from aqueous solution and groundwater by wheat straw, sawdust and activated bagasse carbon of sugarcane. Ecol Eng. 2013;52:211-8. doi: 10.1016/j.ecoleng.2012.12.069.
15. Asgari G, Roshani B, Ghanizadeh G. The investigation of kinetic and isotherm of fluoride adsorption onto functionalize pumice stone. J Hazard Mater. 2012;217-218:123-32. doi: 10.1016/j.jhazmat.2012.03.003.
16. Heibati B, Rodriguez-Couto S, Turan NG, Ozgonenel O, Albadarin AB, Asif M, et al. Removal of noxious dye--Acid Orange 7 from aqueous solution using natural pumice and Fe-coated pumice stone. J Ind Eng Chem. 2015;31:124-31. doi: 10.1016/j.jiec.2015.06.016.
17. Heibati B, Rodriguez-Couto S, Amrane A, Rafatullah M, Hawari A, Al-Ghouti MA. Uptake of Reactive Black 5 by pumice and walnut activated carbon: Chemistry and adsorption mechanisms. J Ind Eng Chem. 2014;20(5):2939-47. doi: 10.1016/j.jiec.2013.10.063.
18. Kim JK, Cheruvally G, Ahn JH. Electrochemical properties of LiFePO4/C synthesized by mechanical activation using sucrose as carbon source. J Solid State Electrochem. 2008;12(7):799-805. doi: 10.1007/s10008-007-0425-y.
19. Zhou Q, Yang JW, Wang YZ, Wu YH, Wang DZ. Preparation of nano-MgO/Carbon composites from sucrose-assisted synthesis for highly efficient dehydrochlorination process. Mater Lett. 2008;62(12-13):1887-9. doi: 10.1016/j.matlet.2007.10.031.
20. Lagergren S. Zur theorie der sogenannten adsorption geloster stoffe, Kungliga Svenska Vetenskapsakademiens. Handlingar. 1898;24:1-39.
21. Ho YS. Second-order kinetic model for the sorption of cadmium onto tree fern: A comparison of linear and non-linear methods. Water Res. 2006;40(1):119-25. doi: 10.1016/j.watres.2005.10.040.
22. Weber WJ Jr, Morris JC. Equilibria and capacities for adsorption on carbon. J Sanit Eng Div. 1964;90(3):79-108.
23. Ghanizadeh G, Asgari G. Adsorption kinetics and isotherm of methylene blue and its removal from aqueous solution using bone charcoal. React Kinet Mech Cat. 2011;102(1):127-42. doi: 10.1007/s11144-010-0247-2.
24. Langmuir I. The constitution and fundamental properties of solids and liquids. Part I. Solids. J Am Chem Soc. 1916;38(11):2221-95. doi: 10.1021/ja02268a002.
25. Ghasemi M, Naushad M, Ghasemi N, Khosravi-fard Y. A novel agricultural waste based adsorbent for the removal of Pb(II) from aqueous solution: Kinetics, equilibrium and thermodynamic studies. J Ind Eng Chem. 2014;20(2):454-61.

doi: 10.1016/j.jiec.2013.05.002.
26. Asgari G, Ramavandi B, Rasuli L, Ahmadi M. Cr (VI) adsorption from aqueous solution using a surfactant-modified Iranian zeolite: characterization, optimization, and kinetic approach. Desalination Water Treat. 2013;51(31-33):6009-20. doi: 10.1080/19443994.2013.769928.
27. Agarwal S, Gupta VK, Ghasemi M, Azimi-Amin J. Peganum harmala-L Seeds adsorbent for the rapid removal of noxious brilliant green dyes from aqueous phase. J Mol Liq. 2017;231:296-305. doi: 10.1016/j.molliq.2017.01.097.
28. Ramavandi B, Asgari G, Faradmal J, Sahebi S, Roshani B. Abatement of Cr (VI) from wastewater using a new adsorbent, cantaloupe peel: Taguchi L16 orthogonal array optimization. Korean J Chem Eng. 2014;31(12):2207-14. doi: 10.1007/s11814-014-0172-6.
29. Luo S, He S, Li X, Sun C, Seshan K. Carbon covered alumina prepared by the pyrolysis of sucrose: A promising support material for the supported Pt–Sn bimetallic dehydrogenation catalysts. Catal Today. 2014;234:295-300. doi: 10.1016/j.cattod.2014.02.010.
30. Ersoy B, Sariisik A, Dikmen S, Sariisik G. Characterization of acidic pumice and determination of its electrokinetic properties in water. Powder Technol. 2010;197(1-2):129-35. doi: 10.1016/j.powtec.2009.09.005.
31. Bedin KC, Martins AC, Cazetta AL, Pezoti O, Almeida VC. KOH-activated carbon prepared from sucrose spherical carbon: Adsorption equilibrium, kinetic and thermodynamic studies for Methylene Blue removal. Chem Eng J. 2016;286:476-84. doi: 10.1016/j.cej.2015.10.099.
32. Noori Sepehr M, Zarrabi M, Kazemian H, Amrane A, Yaghmaian K, Ghaffari HR. Removal of hardness agents, calcium and magnesium, by natural and alkaline modified pumice stones in single and binary systems. Appl Surf Sci. 2013;274:295-305. doi: 10.1016/j.apsusc.2013.03.042.
33. Li Y, Zhang P, Du Q, Peng X, Liu T, Wang Z, et al. Adsorption of fluoride from aqueous solution by graphene. J Colloid Interface Sci. 2011;363(1):348-54. doi: 10.1016/j.jcis.2011.07.032.
34. Asgari G, Dayari A, Ghasemi M, Seid-mohammadi A, Gupta VK, Agarwal S. Efficient fluoride removal by preparation, characterization of pyrolysis bone: Mixed level design experiment and Taguchi L8 orthogonal array optimization, Journal of Molecular Liquids 275 (2019) 251–264. doi: 10.1016/j.molliq.2018.10.137.
35. Mourabet M, El Rhilassi A, El Boujaady H, Bennani-Ziatni M, El Hamri R, Taitai A. Removal of fluoride from aqueous solution by adsorption on hydroxyapatite (HAp) using response surface methodology. J Saudi Chem Soc. 2015;19(6):603-15. doi: 10.1016/j.jscs.2012.03.003.
36. Srivastav AL, Singh PK, Srivastava V, Sharma YC. Application of a new adsorbent for fluoride removal from aqueous solutions. J Hazard Mater. 2013;263 Pt 2:342-52. doi: 10.1016/j.jhazmat.2013.04.017.
37. Biswas K, Gupta K, Ghosh UC. Adsorption of fluoride by hydrous iron(III)–tin(IV) bimetal mixed oxide from the aqueous solutions. Chem Eng J. 2009;149(1-3):196-206. doi: 10.1016/j.cej.2008.09.047.
38. Ali I, Alothman ZA, Sanagi MM. Green synthesis of iron nano-impregnated adsorbent for fast removal of fluoride from water. J Mol Liq. 2015;211:457-65. doi: 10.1016/j.molliq.2015.07.034.
39. Mohan D, Kumar S, Srivastava A. Fluoride removal from ground water using magnetic and nonmagnetic corn stover biochars. Ecol Eng. 2014;73:798-808. doi: 10.1016/j.ecoleng.2014.08.017.